mathematics

MDPI

Article

An Efficient Numerical Method for Fractional SIR Epidemic Model of Infectious Disease by Using Bernstein Wavelets

Sunil Kumar [1], Ali Ahmadian [2], Ranbir Kumar [1], Devendra Kumar [3], Jagdev Singh [4,*], Dumitru Baleanu [5,6] and Mehdi Salimi [7]

1 Department of Mathematics, National Institute of Technology, Jamshedpur 831014, Jharkhand, India; skiitbhu28@gmail.com or skumar.math@nitjsr.ac.in (S.K.); ranbir.iitkgpian@gmail.com (R.K.)
2 Institute of Industry Revolution 4.0, National University of Malaysia, UKM Bangi 43600, Selangor, Malaysia; ahmadian.hosseini@gmail.com
3 Department of Mathematics, University of Rajasthan, Jaipur 302004, Rajasthan, India; devendra.maths@gmail.com
4 Department of Mathematics, JECRC University, Jaipur 303905, Rajasthan, India
5 Department of Mathematics, Faculty of Arts and Sciences, Cankaya University, Eskisehir Yolu 29. Km, Yukarıyurtcu Mahallesi Mimar Sinan Caddesi No: 4, 06790 Etimesgut, Turkey; dumitru@cankaya.edu.tr
6 Institute of Space Sciences, 077125 Magurele-Bucharest, Romania
7 Center for Dynamics and Institute for Analysis, Department of Mathematics, Technische Universität Dresden, 01069 Dresden, Germany; mehdi.salimi@tu-dresden.de or msalimi1@yahoo.com
* Correspondence: jagdevsinghrathore@gmail.com; Tel.: +91-9460905224

Received: 14 March 2020; Accepted: 7 April 2020; Published: 10 April 2020

Abstract: In this paper, the operational matrix based on Bernstein wavelets is presented for solving fractional SIR model with unknown parameters. The SIR model is a system of differential equations that arises in medical science to study epidemiology and medical care for the injured. Operational matrices merged with the collocation method are used to convert fractional-order problems into algebraic equations. The Adams–Bashforth–Moulton predictor correcter scheme is also discussed for solving the same. We have compared the solutions with the Adams–Bashforth predictor correcter scheme for the accuracy and applicability of the Bernstein wavelet method. The convergence analysis of the Bernstein wavelet has been also discussed for the validity of the method.

Keywords: Bernstein wavelets; operational matrix; fractional differential equations; Adams–Bashforth–Moulton predictor correcter scheme

1. Introduction

The construction of mathematical models for real-world phenomena and development of efficacious techniques to define them is one of the most critical issues in applied mathematics biology, engineering, physics and other fields of science. In the 19th century, SIR epidemiological was first introduced by Kermack et al. [1]. In an SIR epidemic model, the population has three components, those susceptible (S), those infected (I) and those recovered (R) from the disease [1]. Presently childhood diseases are most significant infectious diseases. Rubella, measles, poliomyelitis, and hepatitis B have serious concerns among them [2–7]. Recently, coronavirus diseases have been discussed in [8]. Mathematical models play a key role in analyzing the mechanism of transmission of disease and provide different approaches to control the propagation of disease. In the current article, we examine the subsequent mathematical model of arbitrary order:

$$\begin{cases} {}_0^C D_\tau^\sigma S(\tau) = -p_1 S(\tau) I(\tau), \\ {}_0^C D_\tau^\sigma I(\tau) = p_1 S(\tau) I(\tau) - p_2 I(\tau), \\ {}_0^C D_\tau^\sigma R(\tau) = p_2 I(\tau). \end{cases} \tag{1}$$

The associated initial conditions (ICs) are given as $S(0) = S_0$, $I(0) = I_0$ and $R(0) = R_0$.

Bernstein polynomials (BP) were suggested by Sergei Natanovich Bernstein in 1912 which is a polynomial in the Bernstein form that is a linear combination of Bernstein basis polynomials. There are several research articles on Bernstein polynomial for solving fractional differential equations [9–11].

Wavelet theory is a relatively incipient and dominating area in research and innovation. Wavelets have been used in numerous fields such as image compression, signal processing, time frequency analysis, data compression and fast algorithm for easy implementation [12,13]. Wavelet sanctions the precise depiction of a variety of functions and operators [14,15]. Recently, many research papers are published on different types of wavelets, the aim of these research papers to provide the numerical solutions to differential equations of integer order as well as fractional order with the aid of wavelets [16–21]. Recently, Boonrod and Razzaghi discussed a numerical approach based on Legendre wavelets for examining fractional differential equations (FDEs) by the exact formula for Riemann–Liouville (RL) [22]. Rahimkhani and Ordokhani discussed a numerical scheme for solving FDEs by Bernoulli wavelets [23]. Recently several other analytical and numerical schemes have been used to examine fractional order models [24–26].

The key aim of present investigation is to a discuss an efficient computational approach for solving Equation (1). The suggested computational approach is based upon Bernstein wavelets approximation. An exact formula for the RL fractional integral operator for the Bernstein wavelets is computed. Moreover, the derived formula is then employed to convert the linear or non-linear fractional differential equations into the system of algebraic equations. Next, Adams–Bashforth predictor correcter scheme is also discussed for solving the same [27,28]. We have compared the solutions with Adams–Bashforth predictor correcter scheme for the accuracy and applicability of the Bernstein wavelets technique.

The rest of paper is presented as follows: Some results, basic definitions and fractional calculus (FC) are provided in Section 2 which are used in the proposed work. The basic idea of normalized Bernstein wavelets and its properties are presented in Section 3 which is base of proposed work. In Section 4, a Bernstein wavelet operational matrix using Riemann−Liouville integral operator is discussed and presented. In Section 5, we presented convergence and error analysis theorem on Bernstein wavelets. In Section 6, we have implemented Bernstein wavelets and Adam's-Bashforth-Moulton methods. Numerical results and discussions for the fractional SIR epidemic model are completely discussed in Section 7 which is main part of the proposed work.

2. Fractional Calculus

This part presents some preliminaries and notations of FC. There are numerous definitions of derivative and integration are available in litrature [29–41]. It is well known by the several published research papers that the Caputo and RL definitions are most popular definition of fractional calculus.

Definition 1. *The (left sided) RL fractional integral of order $\sigma > 0$ of a function $\Upsilon(\tau) \in C_\sigma, \sigma \geq -1$ is expressed as,*

$$I_\tau^\sigma \Upsilon(\tau) = \frac{1}{\Gamma(\sigma)} \int_0^\tau (\tau - \xi)^{\sigma - 1} \Upsilon(\xi) d\xi, \ \sigma > 0, \tau > 0. \tag{2}$$

In the above equation $\Gamma(.)$ is indicating the famous Gamma function.

Definition 2. *The following two Eqs. presents the RL and Caputo fractional derivatives of order a, respectively,*

$$
{}_{0}^{RL}D_{\tau}^{\sigma}\Upsilon(\tau) = \frac{d^m}{d\tau^m}\left(I_{\tau}^{m-\sigma}\Upsilon(\tau)\right) = \begin{cases} \frac{d^m\Upsilon(\tau)}{d\tau^m}, & \alpha = m \in N, \\ \frac{1}{\Gamma(m-\sigma)}\frac{d^m}{d\tau^m}\int\limits_0^{\tau}\frac{\Upsilon(\xi)}{(\tau-\xi)^{\sigma-m+1}}d\xi, & 0 \le m-1 < \sigma < m, \end{cases}
$$

and,

$$
{}_{0}^{C}D_{\tau}^{\sigma}\Upsilon(\tau) = I_{\tau}^{m-\sigma}\left(\frac{d^m}{d\tau^m}\Upsilon(\tau)\right) = \begin{cases} \frac{d^m\Upsilon(\tau)}{d\tau^m}, & \alpha = m \in N, \\ \frac{1}{\Gamma(m-\sigma)}\int\limits_0^{\tau}\frac{\Upsilon^m(\xi)}{(\tau-\xi)^{\sigma-m+1}}d\xi, & 0 \le m-1 < \sigma < m, \end{cases}
$$

where $\tau > 0$ and m is an integer. It has the following two basic properties for $m-1 < \alpha \le m$ and $\Upsilon \in L_1[a,b]$,

$$
\begin{cases} ({}_{0}^{C}D_{\tau}^{\sigma}I_{\tau}^{\sigma}\Upsilon)(\tau) = \Upsilon(\tau), \\ (I_{\tau}^{\sigma}\,{}_{0}^{C}D^{\sigma}\Upsilon)(\tau) = \Upsilon(\tau) - \sum_{k=0}^{m-1}\Upsilon^k(0^+)\frac{(\tau-a)^k}{k!}. \end{cases} \tag{3}
$$

3. The Normalized Bernstein Wavelets and Its Properties

In the present section, we construct Bernstein wavelet using the orthonormal Bernstein polynomial. Some important properties of Bernstein wavelets are considered in this section.

A family of wavelet functions build up from dilation and translation of a single function ψ are constituted wavelets. if the dilation parameter ρ and the translation parameter δ are continuous, the family of continuous wavelets is presented as

$$
\psi_{\rho\delta}(\tau) = \mid \rho \mid^{-\frac{1}{2}}\,\psi\left(\frac{\tau-\delta}{\rho}\right), \quad \rho,\delta \in \mathbb{R}, \rho \neq 0.
$$

If it is restricted that the parameters a and b take discrete values as $\rho = \rho_0^{-k}$, $\delta = nb_0\rho_0^{-k}$, $\rho_0 > 1$, $\delta_0 > 0$, then we get the subsequent family of discrete wavelets,

$$
\psi_{kn}(\tau) = \mid \rho \mid^{\frac{k}{2}}\,\psi(\rho_0^k - n\delta_0), \quad k,n \in \mathbb{Z},
$$

where the sequence ψ_{kn} form a wavelet basis for $L^2(R)$, and if $\rho_0 = 2$ and $\delta_0 = 1$ then we have an orthonormal basis.

The aforesaid Bernstein wavelet $\psi_{nm}(\tau) = \psi(k,n,m,\tau)$ have four parameters, defined over $[0,1]$ by,

$$
\psi_{nm}(\tau) = \begin{cases} 2^{k/2}\mathcal{B}_{m,M}(2^k\tau - n), & if, \frac{n}{2^k} \le \tau < \frac{n+1}{2^k}, \\ 0, & otherwise, \end{cases} \tag{4}
$$

where $n = 0,1,\ldots,2^k-1$, $m = 0,1,\ldots,\mathcal{M}$, τ is the normalized time and m is the degree of the orthonormal Bernstein polynomial. Furthermore,

$$
\mathcal{B}_{m,\mathcal{M}}(\tau) = (\sqrt{2(\mathcal{M}-m)+1})(1-\tau)^{\mathcal{M}-m}\sum_{i=0}^{m}(-1)^i\binom{2\mathcal{M}+1-i}{m-i}\binom{m}{i}\tau^{m-i}. \tag{5}
$$

or,

$$\mathcal{B}_{m,\mathcal{M}}(\tau) = (\sqrt{2(\mathcal{M}-m)+1})\sum_{i=0}^{m}(-1)^i \frac{\binom{2\mathcal{M}+1-i}{m-i}\binom{m}{i}}{\binom{\mathcal{M}}{m-i}} B_{m-i,\mathcal{M}}(\tau). \tag{6}$$

Here $B_{m,\mathcal{M}}$ are Bernstein polynomials of degree m defined on the interval $[0,1]$ as follows,

$$B_{m,\mathcal{M}}(\tau) = \binom{\mathcal{M}}{m}\tau^m(1-\tau)^{\mathcal{M}-m},\ \ m = 0,1,2,\ldots,\mathcal{M}. \tag{7}$$

$$B_{m,\mathcal{M}}(\tau) = \sum_{j=m}^{\mathcal{M}}(-1)^{j-m}\binom{\mathcal{M}}{m}\binom{\mathcal{M}-m}{j-m}\tau^j,\ m = 0,1,2,\ldots,\mathcal{M}. \tag{8}$$

or,

$$B_{m,\mathcal{M}}(1-\tau) = \binom{\mathcal{M}}{m}(1-\tau)^m\tau^{(\mathcal{M}-m)}.$$

Furthermore, we replace m by $\mathcal{M}-m$, we get

$$B_{\mathcal{M}-m,\mathcal{M}}(1-\tau) = \binom{\mathcal{M}}{\mathcal{M}-m}(1-\tau)^{\mathcal{M}-m}\tau^m = \binom{\mathcal{M}}{m}(1-\tau)^{\mathcal{M}-m}\tau^m = B_{m,\mathcal{M}}(\tau).$$

Let us assume that the value of symbol $\Delta_{\mathcal{M},m}$ is $\Delta_{\mathcal{M},m} = \binom{\mathcal{M}}{m}$, where $\binom{\mathcal{M}}{m} = \frac{\mathcal{M}!}{m!(\mathcal{M}-m)!}$.

Any function $\Upsilon(\tau)$ defined over $[0,1)$ may be expressed in terms of Bernstein wavelet as

$$\Upsilon(\tau) = \sum_{n=0}^{\infty}\sum_{m\in Z}\Lambda_{nm}\psi_{nm}(\tau), \tag{9}$$

where $\Lambda_{nm} =< \Upsilon, \psi_{nm} >= \int_0^1 \psi_{nm}(\tau)\Upsilon(\tau)d\tau$, with $< .,. >$ as the inner product defined on $L^2[0,1]$. If the infinite series is truncated, then the above Eq. is presented as

$$\Upsilon(\tau) \approx \sum_{n=0}^{2^k-1}\sum_{m=0}^{\mathcal{M}}\Lambda_{nm}\psi_{nm}(\tau) = C^T\Psi(\tau),$$

where T denotes the transposition and, C and $\Psi(\tau)$ are the $\hat{m} = 2^k(\mathcal{M}+1)$ column vectors. $C = [\Lambda_{00}, \Lambda_{01}, \ldots, \Lambda_{0,\mathcal{M}}, \Lambda_{1,0}, \ldots, \Lambda_{1\mathcal{M}}, \Lambda_{(2^k-1)0}, \ldots, \Lambda_{(2^k-1)\mathcal{M}}]^T$ and $\Psi(\tau) = [\psi_{00}, \psi_{01}, \ldots, \psi_{0,\mathcal{M}}, \psi_{1,0}, \ldots, \psi_{1\mathcal{M}}, \psi_{(2^k-1)0}, \ldots, \psi_{(2^k-1)\mathcal{M}}]^T$. Here, we define Bernstein wavelet matrix $\Phi_{\hat{m}\times\hat{m}}$ as

$$\Phi_{\hat{m}\times\hat{m}} = [\Psi(\frac{2i-1}{2\hat{m}})], i = 1,2,\ldots,2^k(\mathcal{M}+1).$$

$$\Phi_{12\times 12} = \left\{ \begin{array}{cccccccccccc} 3.1056 & 1.1180 & 0.1242 & 0 & 0 & 0 & 0 & 0 & 0 & 0 & 0 & 0 \\ 0 & 0 & 0 & 3.1056 & 1.1180 & 0.1242 & 0 & 0 & 0 & 0 & 0 & 0 \\ 0 & 0 & 0 & 0 & 0 & 0 & 3.1056 & 1.1180 & 0.1242 & 0 & 0 & 0 \\ 0 & 0 & 0 & 0 & 0 & 0 & 0 & 0 & 0 & 3.1056 & 1.1180 & 0.1242 \\ -0.4811 & 2.5981 & 1.8283 & 0 & 0 & 0 & 0 & 0 & 0 & 0 & 0 & 0 \\ 0 & 0 & 0 & -0.4811 & 2.5981 & 1.8283 & 0 & 0 & 0 & 0 & 0 & 0 \\ 0 & 0 & 0 & 0 & 0 & 0 & -0.4811 & 2.5981 & 1.8283 & 0 & 0 & 0 \\ 0 & 0 & 0 & 0 & 0 & 0 & 0 & 0 & 0 & -0.4811 & 2.5981 & 1.8283 \\ -0.1111 & -1.0000 & 2.5556 & 0 & 0 & 0 & 0 & 0 & 0 & 0 & 0 & 0 \\ 0 & 0 & 0 & -0.1111 & -1.0000 & 2.5556 & 0 & 0 & 0 & 0 & 0 & 0 \\ 0 & 0 & 0 & 0 & 0 & 0 & -0.1111 & -1.0000 & 2.5556 & 0 & 0 & 0 \\ 0 & 0 & 0 & 0 & 0 & 0 & 0 & 0 & 0 & -0.1111 & -1.0000 & 2.5556 \end{array} \right\}.$$

The above matrix $\Phi_{\hat{m}\times\hat{m}}$ is Bernstein matrix at given collocation points $\frac{2i-1}{2\hat{m}}$, where $k=2$ and $\mathcal{M}=2$.

4. Bernstein Wavelet Operational Matrix Using Riemann–Liouville Integral Operator

The principal target of this part is to derive the operational matrix for Bernstein wavelet without using block pulse functions. For this, we operate I_τ^α operator directly into $\Psi(\tau)$ as follows

$$I_\tau^\sigma \Psi(\tau) = Q(\tau,\sigma), \tag{10}$$

where

$$Q(\tau,\sigma) = [I_\tau^\sigma \psi_{00}, I_\tau^\sigma \psi_{01}, \ldots, I_\tau^\sigma \psi_{0,\mathcal{M}}, I_\tau^\sigma \psi_{1,0}, \ldots, I_\tau^\sigma \psi_{1\mathcal{M}}, I_\tau^\sigma \psi_{(2^k-1)0}, \ldots, I_\tau^\sigma \psi_{(2^k-1)\mathcal{M}}]^T.$$

$$\psi_{nm}(\tau) = \mu_{\frac{n}{2^k}}(\tau) 2^{k/2} \mathcal{B}_{m,\mathcal{M}}(2^k\tau - n) - \mu_{\frac{n+1}{2^k}}(\tau) 2^{k/2} \mathcal{B}_{m,\mathcal{M}}(2^k\tau - n), \tag{11}$$

where $\mu_a(\tau)$ is the unit step function given as

$$\mu_a(\tau) = \begin{cases} 1, & \tau \geq a, \\ 0, & \tau < a. \end{cases} \tag{12}$$

Here, operating the Laplace transform to calculate $I_\tau^\sigma \psi_{nm}(\tau)$ using Equation (11) for $m = 0,1,\ldots,\mathcal{M}$, $n = 0,1,\ldots,2^k-1$, we have

$$\begin{aligned} \mathcal{L}[\psi_{nm}(\tau)] =& \mathcal{L}[\mu_{\frac{n}{2^k}}(\tau) 2^{k/2} \mathcal{B}_{m,\mathcal{M}}(2^k\tau - n) - \mu_{\frac{n+1}{2^k}}(\tau) 2^{k/2} \mathcal{B}_{m,\mathcal{M}}(2^k\tau - n)], \\ =& \mathcal{L}[\mu_{\frac{n}{2^k}}(\tau) 2^{k/2} \sqrt{2(\mathcal{M}-m)+1} \sum_{i=0}^{m} (-1)^i \frac{\Delta_{2\mathcal{M}+1-i,m-i}\Delta_{m,i}}{\Delta_{\mathcal{M}-i,m-i}} \\ & \times B_{m-i,\mathcal{M}}(2^k(\tau - \frac{n}{2^k})) - \mu_{\frac{n+1}{2^k}}(\tau) 2^{k/2} \sqrt{2(\mathcal{M}-m)+1} \\ & \times \sum_{i=0}^{m} (-1)^i \frac{\Delta_{2\mathcal{M}+1-i,m-i}\Delta_{m,i}}{\Delta_{\mathcal{M}-i,m-i}} B_{\mathcal{M}-m,\mathcal{M}-i}(-2^k(\tau - \frac{n+1}{2^k}))], \end{aligned} \tag{13}$$

$$\begin{aligned}\mathcal{L}[\psi_{nm}(\tau)] =& e^{-\frac{n}{2^k}s}(\tau)2^{k/2}\sqrt{2(\mathcal{M}-m)+1}\sum_{i=0}^{m}(-1)^i\frac{\Delta_{2\mathcal{M}+1-i,m-i}\Delta_{m,i}}{\Delta_{\mathcal{M}-i,m-i}}\\ &\times \mathcal{L}[B_{m-i,\mathcal{M}}(2^k\tau)] - e^{-\frac{n+1}{2^k}s}2^{k/2}\sqrt{2(\mathcal{M}-m)+1}\\ &\times \sum_{i=0}^{m}(-1)^i\frac{\Delta_{2\mathcal{M}+1-i,m-i}\Delta_{m,i}}{\Delta_{\mathcal{M}-i,m-i}}\mathcal{L}[B_{\mathcal{M}-m,\mathcal{M}-i}(-2^k\tau)],\end{aligned} \tag{14}$$

where

$$\begin{aligned}\mathcal{L}[B_{m-i,\mathcal{M}}(2^k\tau)] =& \mathcal{L}[\sum_{j=m-i}^{M-i}(-1)^{j-m+i}\Delta_{\mathcal{M}-i,m-i}\Delta_{\mathcal{M}-m,j-m+i}2^{kj}\tau^j],\\ & \Delta_{\mathcal{M}-m,j-m+i}2^{kj}\frac{\Gamma(j+1)}{s^{j+1}},\\ \mathcal{L}[B_{\mathcal{M}-m,\mathcal{M}-i}(-2^k\tau)] =& \mathcal{L}[\sum_{j=\mathcal{M}-m}^{\mathcal{M}-i}(-1)^{2j-\mathcal{M}+m}\Delta_{\mathcal{M}-i,\mathcal{M}-m}\Omega_{m-i,j-\mathcal{M}+m}2^{kj}\tau^j],\\ =& \sum_{j=\mathcal{M}-m}^{\mathcal{M}-i}(-1)^{2j-\mathcal{M}+m}\Delta_{\mathcal{M}-i,\mathcal{M}-m}\Delta_{m-i,j-\mathcal{M}+m}2^{kj}\frac{\Gamma(j+1)}{s^{j+1}},\end{aligned} \tag{15}$$

$$\mathcal{L}[I_\tau^\sigma\psi_{nm}(\tau)] = \mathcal{L}[\frac{1}{\Gamma(\sigma)\tau^{1-\sigma}} * \psi_{nm}(\tau)] = \mathcal{L}[\frac{1}{\Gamma(\sigma)\tau^{1-\sigma}}]\mathcal{L}[\psi_{nm}(\tau)]. \tag{16}$$

Furthermore, operating the inverse Laplace transform into Equation (16), we get

$$I_\tau^\sigma\psi_{nm}(\tau) = \begin{cases} 0, \ \ if, 0 \le \tau < \frac{n}{2^k}, \\ 2^{k/2}\xi(m,\mathcal{M})(\tau-\frac{n}{2^k})^\sigma, \ \ if \ \frac{n}{2^k} \le \tau < \frac{n+1}{2^k}, \\ 2^{k/2}\xi(m,\mathcal{M})(\tau-\frac{n}{2^k})^\sigma - 2^{k/2}\bar{\xi}(m,\mathcal{M})(\tau-\frac{n+1}{2^k})^\sigma, \ \ if \ \frac{n+1}{2^k} \le \tau < 1, \end{cases} \tag{17}$$

$$\begin{aligned}\xi(m,\mathcal{M}) =& \sqrt{(2(\mathcal{M}-m)+1)}\sum_{i=0}^{m}(-1)^i\frac{\Delta_{2\mathcal{M}+1-i,m-i}\Delta_{m,i}}{\Delta_{\mathcal{M}-i,m-i}}\sum_{j=m-i}^{\mathcal{M}}(-1)^{j-m+i}\\ &\times \Delta_{\mathcal{M}-i,m-i}\Delta_{\mathcal{M}-m,j-m+i}2^{jk}(\tau-\frac{n}{2^k})^j\frac{\Gamma(j+1)}{\Gamma(\sigma+j+1)}\\ \bar{\xi}(m,M) =& \sqrt{(2(\mathcal{M}-m)+1)}\sum_{i=0}^{m}(-1)^i\frac{\Delta_{2\mathcal{M}+1-i,m-i}\Delta_{m,i}}{\Delta_{\mathcal{M}-i,m-i}}\sum_{j=\mathcal{M}-m}^{\mathcal{M}}(-1)^{2j-\mathcal{M}+m}\\ &\times \Delta_{\mathcal{M}-i,\mathcal{M}-m}\Delta_{m-i,j-\mathcal{M}+m}2^{jk}(\tau-\frac{n+1}{2^k})^j\frac{\Gamma(j+1)}{\Gamma(\sigma+j+1)}.\end{aligned}$$

If, we consider the fixed value as $k = 2$, $\mathcal{M} = 2$, $\sigma = 0.5$ and the collocation points $\frac{2i-1}{2\hat{m}}$. However, we get the operational matrix given below

$$Q^{0.5} = \left\{ \begin{array}{cccccccccccc} 0.8164 & 0.8326 & 0.5972 & 0.4490 & 0.3802 & 0.3363 & 0.3050 & 0.2812 & 0.2622 & 0.2467 & 0.2336 & 0.2224 \\ 0 & 0 & 0 & 0.8164 & 0.8326 & 0.5972 & 0.4490 & 0.3802 & 0.3363 & 0.3050 & 0.2812 & 0.2622 \\ 0 & 0 & 0 & 0 & 0 & 0 & 0.8164 & 0.8326 & 0.5972 & 0.4490 & 0.3802 & 0.3363 \\ 0 & 0 & 0 & 0 & 0 & 0 & 0 & 0 & 0 & 0.8164 & 0.8326 & 0.5972 \\ -0.3251 & 0.4607 & 0.8590 & 0.4919 & 0.3703 & 0.3099 & 0.2719 & 0.2451 & 0.2249 & 0.2089 & 0.1960 & 0.1852 \\ 0 & 0 & 0 & -0.3251 & 0.4607 & 0.8590 & 0.4919 & 0.3703 & 0.3099 & 0.2719 & 0.2451 & 0.2249 \\ 0 & 0 & 0 & 0 & 0 & 0 & -0.3251 & 0.4607 & 0.8590 & 0.4919 & 0.3703 & 0.3099 \\ 0 & 0 & 0 & 0 & 0 & 0 & 0 & 0 & 0 & -0.3251 & 0.4607 & 0.8590 \\ 0.1194 & -0.2660 & 0.2671 & 0.4183 & 0.2608 & 0.2045 & 0.1735 & 0.1532 & 0.1387 & 0.1277 & 0.1189 & 0.1117 \\ 0 & 0 & 0 & 0.1194 & -0.2660 & 0.2671 & 0.4183 & 0.2608 & 0.2045 & 0.1735 & 0.1532 & 0.1387 \\ 0 & 0 & 0 & 0 & 0 & 0 & 0.1194 & -0.2660 & 0.2671 & 0.4183 & 0.2608 & 0.2045 \\ 0 & 0 & 0 & 0 & 0 & 0 & 0 & 0 & 0 & 0.1194 & -0.2660 & 0.2671 \end{array} \right\}.$$

The above square matrix $Q^{0.5}$ is operational matrix based on Bernstein wavelet at $\sigma = 0.5$. However, we can also find Bernstein operational wavelet matrix for arbitrary $0 < \sigma \leq 1$.

5. Convergence and Error Analysis

Theorem 1. *The solution obtained by Bernstein wavelets method is converges.*

Proof. Since Bernstein wavelets in Equation (4) forms an orthonormal basis.

Let $\Upsilon(\tau) = \sum_{i=0}^{M-1} \Lambda_{ni}\psi_{ni}(\tau)$ for fixed value of $n \in \mathbb{N}$, where $\Lambda_{ni} =< u(\tau), \psi_{ni}(\tau) >$. Let sequence of partial sums of $\{\Lambda_{ni}\psi_{ni}\}_{n=0}^{\mathcal{M}-1}$ be P_n and P_m defined as $P_n = \sum_{i=0}^{n} \Lambda_{ni}\psi_{ni}(\tau)$ and $P_m = \sum_{i=0}^{m} \Lambda_{ni}\psi_{ni}(\tau)$. Now

$$\begin{aligned} < \Upsilon(\tau), P_n > &= \Big\langle \Upsilon(\tau), \sum_{i=0}^{n} \Lambda_{ni}\psi_{ni}(\tau) \Big\rangle \\ &= \sum_{i=0}^{n} \bar{\Lambda}_{ni} \Big\langle \Upsilon(\tau), \psi_{ni}(\tau) \Big\rangle \\ &= \sum_{i=0}^{n} \bar{\Lambda}_{ni}\Lambda_{ni} \\ &= \sum_{i=0}^{n} |\Lambda_{ni}|^2. \end{aligned}$$

Consequently,

$$\begin{aligned} \Big\| P_n - P_m \Big\|^2 &= \Big\| \sum_{i=0}^{n} \Lambda_{ni}\psi_{ni}(\tau) - \sum_{i=0}^{m} \Lambda_{ni}\psi_{ni}(\tau) \Big\|^2 \\ &= \Big\| \sum_{i=m+1}^{n} \Lambda_{ni}\psi_{ni}(\tau) \Big\|^2 \\ &= \Big\langle \sum_{i=m+1}^{n} \Lambda_{ni}\psi_{ni}(\tau), \sum_{i=m+1}^{n} \Lambda_{ni}\psi_{ni}(\tau) \Big\rangle \\ &= \sum_{i=m+1}^{n} |\Lambda_{ni}|^2. \end{aligned}$$

When $n \to \infty$, $\sum_{i=0}^{\infty} |\Lambda_{ni}|^2$ is convergent by Bessel's inequality. Hence, P_n is Cauchy's sequence converges to P (say). Therefore,

$$
\begin{aligned}
< P - \Upsilon(\tau), \psi_{ni}(\tau) > &= < P, \psi_{ni}(\tau) > - < \Upsilon(\tau), \psi_{ni}(\tau) > \\
&= < P, \psi_{ni}(\tau) > - < lim_{n\to\infty} P_n, \psi_{ni}(\tau) > \\
&= 0.
\end{aligned}
$$

Thus, series solution of the Bernstein wavelets is convergent. □

Theorem 2. *Let $\Upsilon(\tau) \in C^{M+1}[0,1]$ and $P_{\mathcal{M}}^{2^k-1}\Upsilon(\tau)$, where $P_{\mathcal{M}}^{2^k-1}\Upsilon(\tau) = \sum_{n=0}^{2^k-1}\sum_{m=0}^{M} c_{n,m}\psi_{n,m}(\tau)$ is the approximate solution using the Bernstein wavelets then error bound would be given as*

$$
\|\epsilon(\tau)\| \leq \left\| \frac{\rho}{(\mathcal{M}+1)!2^{(\mathcal{M}+1)(K+1)-1}} \right\|,
$$

where $\epsilon(\tau) = |\Upsilon(\tau) - \sum_{n=0}^{2^k-1}\sum_{m=0}^{\mathcal{M}} c_{n,m}\psi_{n,m}(\tau)|$ and $\rho = Max_{\tau\in[0,1)}|\Upsilon^{\mathcal{M}+1}(\tau)|$.

Proof. In view of the concept of norm in inner product space, we have

$$
\|\epsilon(\tau)\|^2 = \int_0^1 \left|\Upsilon(\tau) - P_{\mathcal{M}}^{2^k-1}\Upsilon(\tau)\right|^2 d\tau.
$$

Now, dividing into the 2^k sub-intervals $I_n = \left[\frac{n}{2^k}, \frac{n+1}{2^k}\right]$, $n = 0, 1, 2, \ldots, 2^k - 1$.

$$
\begin{aligned}
\|\epsilon(\tau)\|^2 &= \sum_{n=0}^{2^k-1} \int_{\frac{n}{2^k}}^{\frac{n+1}{2^k}} \left|\Upsilon(\tau) - P_{\mathcal{M}} M^{2^k-1}\Upsilon(\tau)\right|^2 d\tau, \\
\|\epsilon(\tau)\|^2 &= \sum_{n=0}^{2^k-1} \int_{\frac{n}{2^k}}^{\frac{n+1}{2^k}} \left|\Upsilon(\tau) - p_{\mathcal{M}+1}(\tau)\right|^2 d\tau,
\end{aligned}
$$

where $p_{M+1}(\tau)$ is the interpolating polynomial of $\mathcal{M}+1$ degree which approximate $\Upsilon(\tau)$ on the interval I_n. With the aid of the maximum error estimate for the polynomial on I_n, we obtain

$$
\begin{aligned}
\|\epsilon(\tau)\|^2 &\leq \sum_{n=0}^{2^k-1} \int_{\frac{n}{2^k}}^{\frac{n+1}{2^k}} \left| \frac{Max_{\tau\in L^2[0,1)}|\Upsilon^{\mathcal{M}+1}(\tau)}{(\mathcal{M}+1)!2^{(\mathcal{M}+1)(K+1)-1}} \right|^2 d\tau, \\
\|\epsilon(\tau)\|^2 &\leq \sum_{n=0}^{2^k-1} \int_{\frac{n}{2^k}}^{\frac{n+1}{2^k}} \left| \frac{\rho}{(\mathcal{M}+1)!2^{(\mathcal{M}+1)(K+1)-1}} \right|^2 d\tau, \\
\|\epsilon(\tau)\|^2 &\leq \int_0^1 \left| \frac{\rho}{(\mathcal{M}+1)!2^{(\mathcal{M}+1)(K+1)-1}} \right|^2 d\tau.
\end{aligned}
$$

Hence,

$$
\|\epsilon(\tau)\| \leq \left\| \frac{\rho}{(\mathcal{M}+1)!2^{(\mathcal{M}+1)(K+1)-1}} \right\|.
$$

□

6. Proposed Methods for Fractional SIR Epidemic Model

6.1. Bernstein Wavelets for the Numerical Solution of SIR Epidemic Model

Consider the SIR epidemic model (1), we assume higher fractional derivatives in terms of the Bernstein wavelets as

$$\begin{cases} {}_0^C D_\tau^\sigma S(\tau) = A_1^T \Psi(\tau), \\ {}_0^C D_\tau^\sigma I(\tau) = A_2^T \Psi(\tau), \\ {}_0^C D_\tau^\sigma R(\tau) = A_3^T \Psi(\tau). \end{cases} \tag{18}$$

where $A_r^T = [\Lambda_{00}^r, \Lambda_{01}^r, \ldots, \Lambda_{0,\mathcal{M}}^r, \Lambda_{1,0}^r, \ldots, \Lambda_{1\mathcal{M}}^r, \Lambda_{(2^k-1)0}^r, \ldots, \Lambda_{(2^k-1)\mathcal{M}}^r]$ are the unknowns and $r = 1, 2, 3$. Now, we operate fractional integral operator into Equation (18) in the sense of Riemann–Liouville, we obtain

$$\begin{cases} (I_\tau^\sigma {}_0^C D_\tau^\sigma)(S(\tau)) = A_1^T Q(\tau, \sigma), \\ (I_\tau^\sigma {}_0^C D_\tau^\sigma)(I(\tau)) = A_2^T Q(\tau, \sigma), \\ (I_\tau^\sigma {}_0^C D_\tau^\sigma)(R(\tau)) = A_3^T Q(\tau, \sigma). \end{cases} \tag{19}$$

also,

$$\begin{cases} (I_\tau^\sigma {}_0^C D_\tau^\sigma)(S(\tau)) = S(\tau) - S(0) = A_1^T Q(\tau, \sigma), \\ (I_\tau^\sigma {}_0^C D_\tau^\sigma)(I(\tau)) = I(\tau) - I(0) = A_2^T Q(\tau, \sigma), \\ (I_\tau^\sigma {}_0^C D_\tau^\sigma)(R(\tau)) = R(\tau) - R(0) = A_3^T Q(\tau, \sigma). \end{cases} \tag{20}$$

Then

$$\begin{cases} S(\tau) = S(0) + A_1^T Q(\tau, \sigma), \\ I(\tau) = I(0) + A_2^T Q(\tau, \sigma), \\ R(\tau) = R(0) + A_3^T Q(\tau, \sigma), \end{cases} \tag{21}$$

where only A_r^T are unknowns. Putting these values of S, I and R into the main Equation (1) and using the collocation points $\frac{2i-1}{2\hat{m}}$, where $i = 1, 2, \ldots, 2^k(\mathcal{M}+1)$, we can get the system of non-linear algebraic equations with $3\hat{m}$ number unknowns. By solving these equations with the avail of the Newton iteration method by MATLAB software, we can ascertain the unknown Bernstein coefficients. By superseding unknown coefficients into Equation (21), we may obtain the desired solutions.

6.2. Adams–Bashforth–Moulton (ABM) Predictor Corrector Scheme for the Numerical Solution of SIR Epidemic Model

On applying Adam's-Bashforth-Moulton method on Equation (1) we obtained the predictor values and the corresponding corrector values as follows. To change it into discrete form, let $h = \frac{1-0}{\hat{m}}$, $\tau_n = nh$, $n = 0, 1, 2, \ldots, \hat{m} - 1$,

$$
\begin{aligned}
S_{n+1} =& S(0) + \frac{h^{\sigma}}{\Gamma(\sigma+2)}(-p_1 S^p_{n+1} I^p_{n+1}) + \frac{h^{\sigma}}{\Gamma(\sigma+2)} \sum_{j=0}^{n} \alpha_{j,n+1}(-p_1 S_j I_j),\\
I_{n+1} =& I(0) + \frac{h^{\sigma}}{\Gamma(\sigma+2)}(p_1 S^p_{n+1} I^p_{n+1} - p_2 I^p_{n+1}) + \frac{h^{\sigma}}{\Gamma(\sigma+2)} \sum_{j=0}^{n} \alpha_{j,n+1}(p_1 S_j I_j - p_2 I_j),\\
R_{n+1} =& R(0) + \frac{h^{\sigma}}{\Gamma(\sigma+2)}(p_2 I^p_{n+1}) + \frac{h^{\sigma}}{\Gamma(\sigma+2)} \sum_{j=0}^{n} \alpha_{j,n+1}(p_2 I_j),\\
S^p_{n+1} =& S(0) + \frac{1}{\Gamma(\sigma)} \sum_{j=0}^{n} \beta_{j,n+1}(-p_1 S_j I_j),\\
I^p_{n+1} =& I(0) + \frac{1}{\Gamma(\sigma)} \sum_{j=0}^{n} \beta_{j,n+1}(p_1 S_j I_j - p_2 I_j),\\
R^p_{n+1} =& R(0) + \frac{1}{\Gamma(\sigma)} \sum_{j=0}^{n} \beta_{j,n+1}(p_2 I_j),
\end{aligned}
$$

where

$$
\alpha_{j,n+1} = \begin{cases} n^{\sigma+1} - (n-\sigma)(n+1)^{\sigma}, \quad if \;\; j = 0, \\ (n-j+2)^{\sigma+1} + (n-j)^{\sigma+1} - 2(n-j+1)^{\sigma+1}, \quad if \;\; 0 \le j \le n, \\ 1, \quad if \;\; j = 1, \end{cases}
$$

$$
\beta_{j,n+1} = \frac{h^{\sigma}}{\alpha}((n+1-j)^{\sigma} - (n-j)^{\sigma}), \;\; 0 \le j \le n.
$$

7. Numerical Results and Discussion

Here, we obtain the numerical results for fractional SIR epidemic model 1 to verify the applicability and efficiency of the Bernstein wavelets.

$$
\begin{cases} {}^{C}_{0}D^{\sigma}_{\tau} S(\tau) = -0.001 S(\tau) I(\tau), \\ {}^{C}_{0}D^{\sigma}_{\tau} I(\tau) = 0.001 S(\tau) I(\tau) - 0.072 I(\tau), \\ {}^{C}_{0}D^{\sigma}_{\tau} R(\tau) = 0.072 I(\tau), \end{cases} \tag{22}
$$

with initial conditions $S(0) = 620$, $I(0) = 10$ and $R(0) = 70$. Furthermore, we use aforesaid operational matrix to convert system of non-linear FDEs into the system of algebraic equations. To show the validity of the Bernstein wavelets, we compared the obtained solutions with the solutions obtained by Adam's-Bashforth-Moulton methods (ABM). When $M = 2$ and $k = 5$, it is obvious from Figures 1–3 that the obtained solutions by the Bernstein wavelet scheme has an excellent agreement with the ABM.

Moreover, we have obtained relative error and absolute error between solutions obtained by both methods, where relative error and absolute error is defined as

$$Rel(\tau_i) = \left|\frac{ABM(\tau_i) - BWM(\tau_i)}{ABM(\tau_i)}\right|. \tag{23}$$

and

$$Abs(\tau_i) = \left|ABM(\tau_i) - BWM(\tau_i)\right|. \tag{24}$$

Relative error and absolute error are depicted through Figures 4–9. Consequently, we have shown the effect of fractional derivative on the SIR model. From Figures 10–12, it is clear that the fractional derivative gives more freedom compare to integer order derivative, by the proposed method we are able to find the solutions for arbitrary order of derivative. From Figures 13–15 we have shown the 3D plot of the susceptible, infected and recovered people. In Tables 1–3, we have compared the obtained solutions with RK4 and RPS numerical methods, we found that our solutions are convergent. If we increase the values of M and k we can obtain more appropriate results compare to another numerical methods.

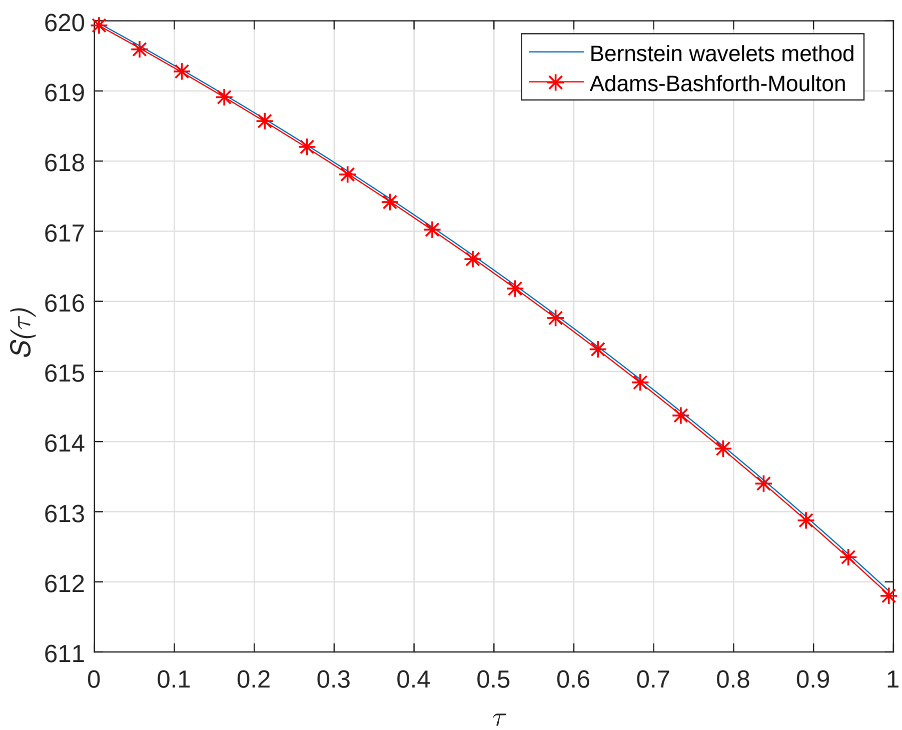

Figure 1. Plot of susceptible people w.r.t time at $\sigma = 1$ by Bernstein wavelets method.

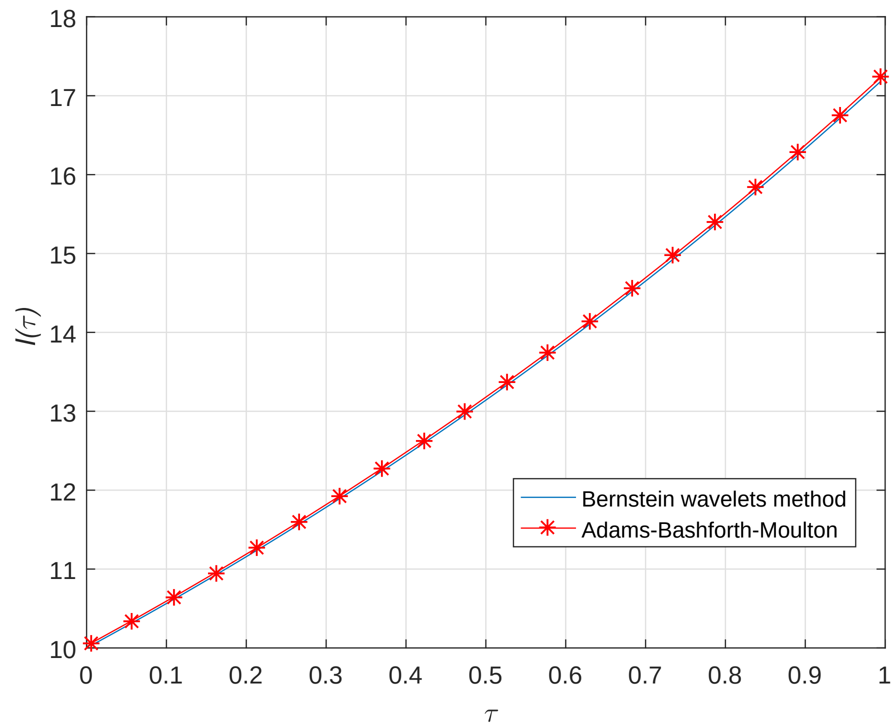

Figure 2. Plot of infected people w.r.t time at $\sigma = 1$ by Bernstein wavelets method.

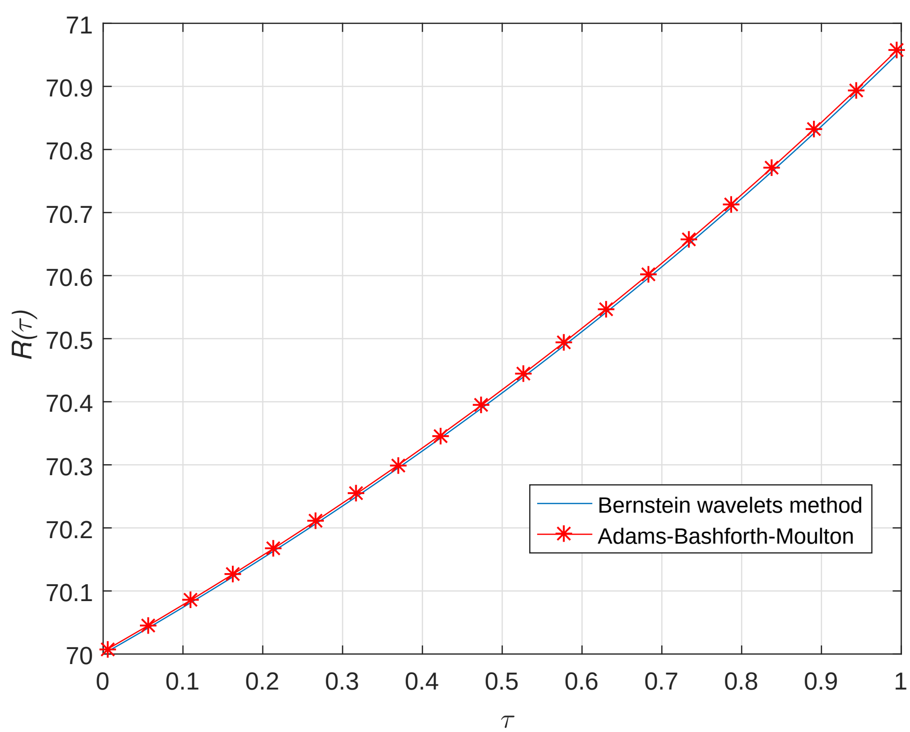

Figure 3. Plot of recovered people w.r.t time at $\sigma = 1$ by Bernstein wavelets method.

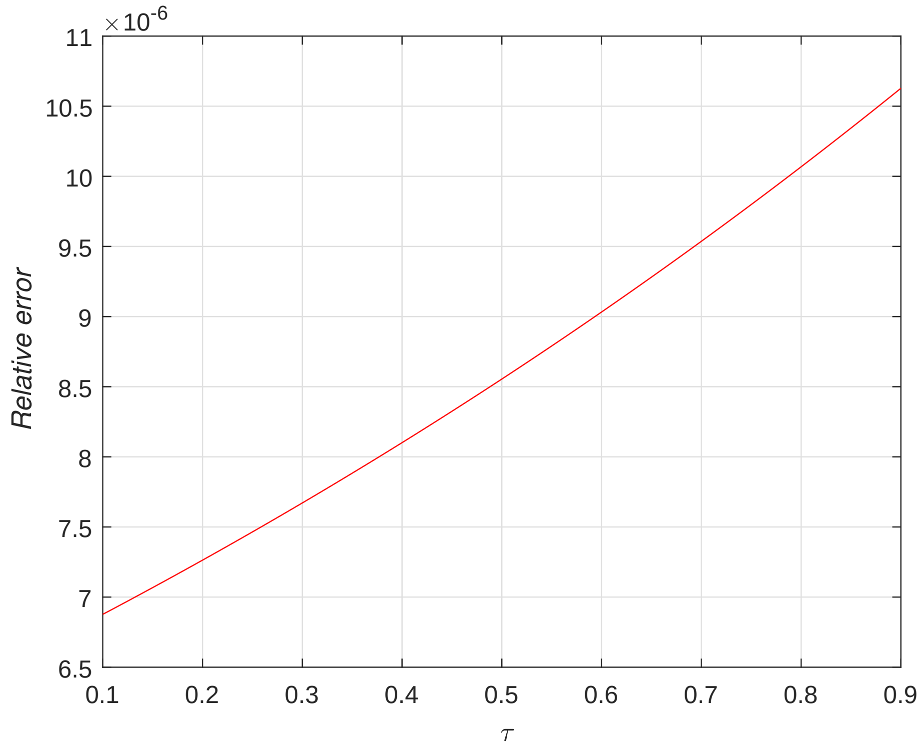

Figure 4. Relative error between obtained solutions by BWM and ABM.

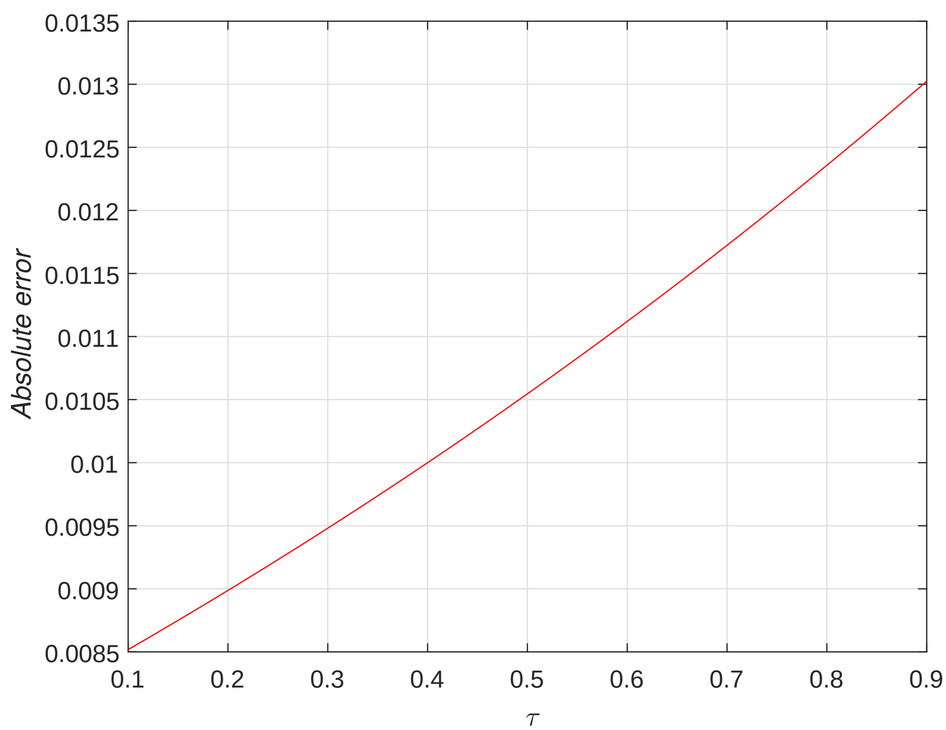

Figure 5. Absolute error between obtained solutions by BWM and ABM.

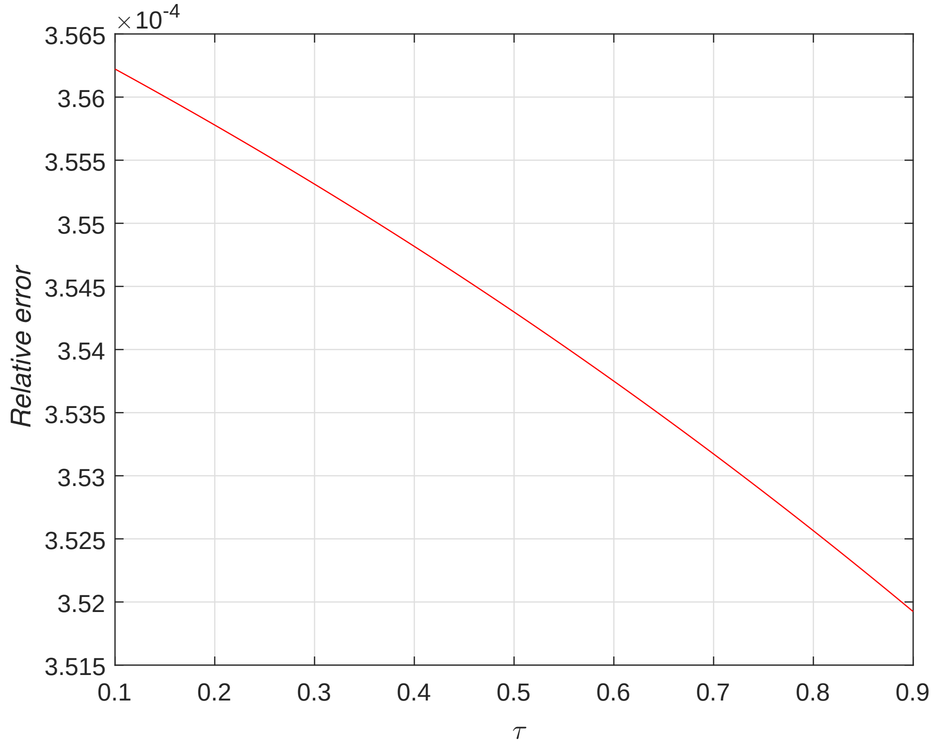

Figure 6. Relative error between obtained solutions by BWM and ABM.

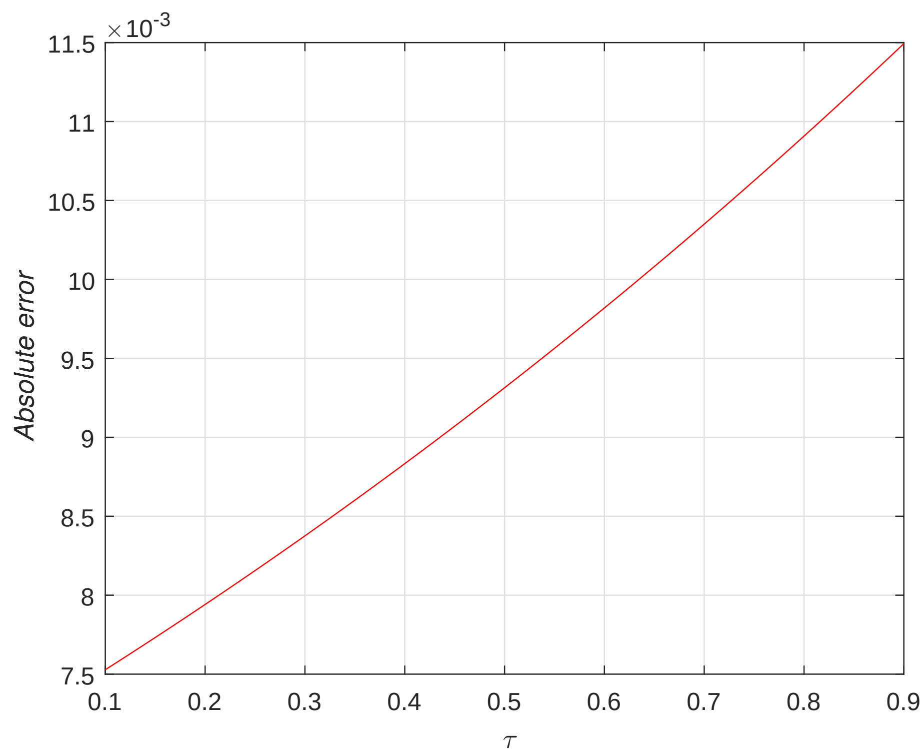

Figure 7. Absolute error between obtained solutions by BWM and ABM.

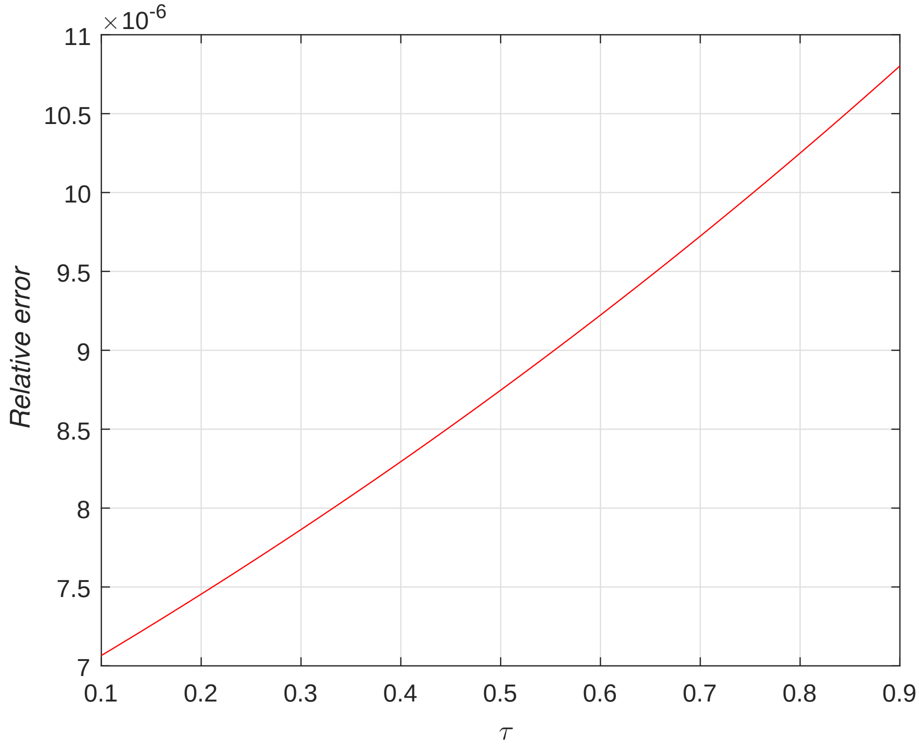

Figure 8. Relative error between obtained solutions by BWM and ABM.

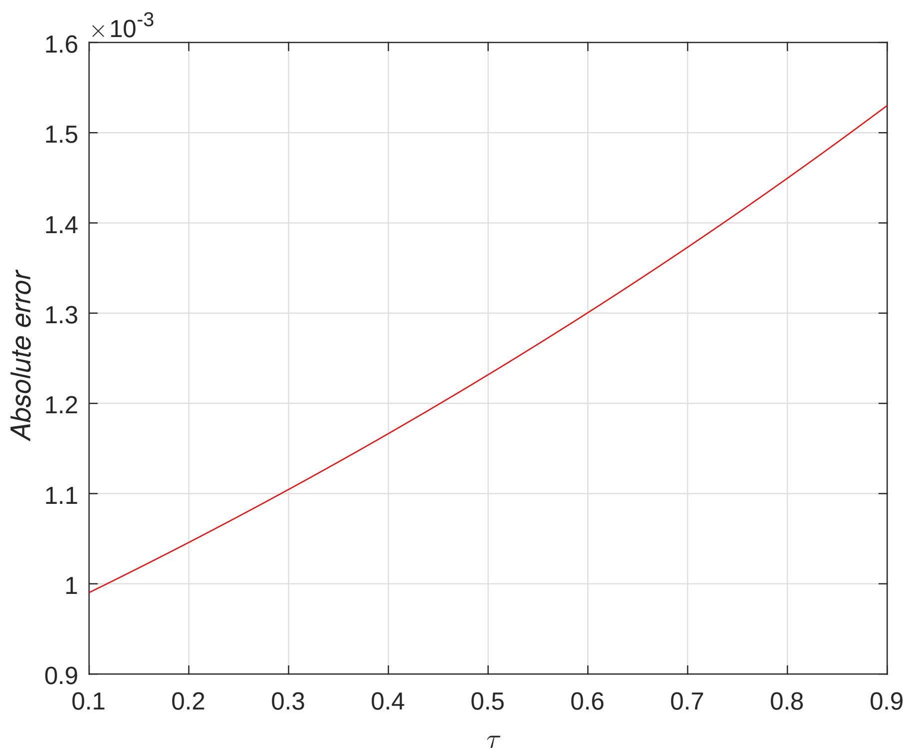

Figure 9. Absolute error between obtained solutions by BWM and ABM.

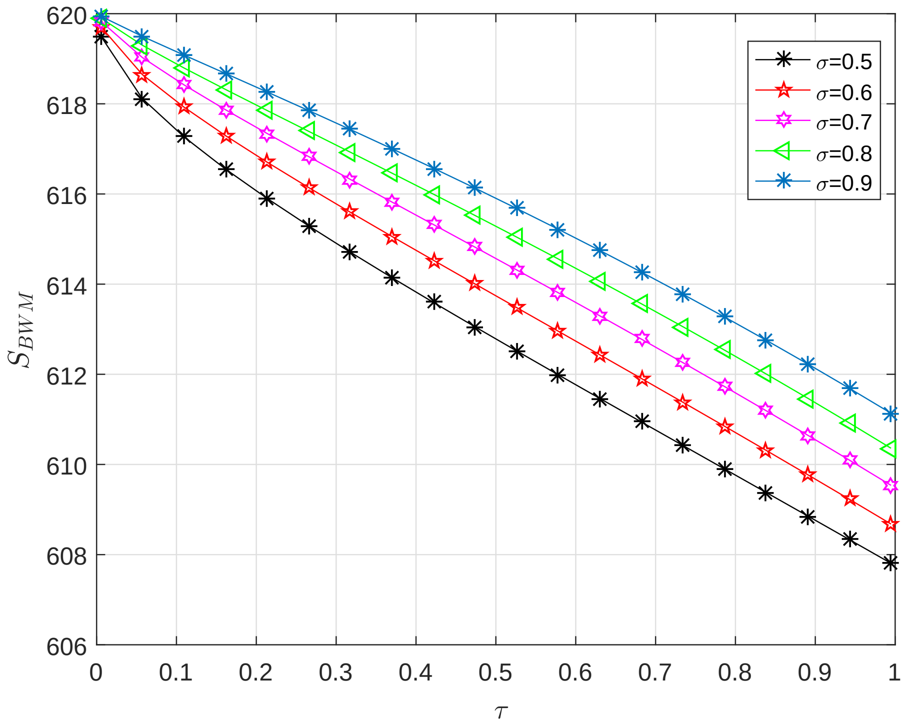

Figure 10. Behavior of Susceptible people w.r.t time for different values of σ.

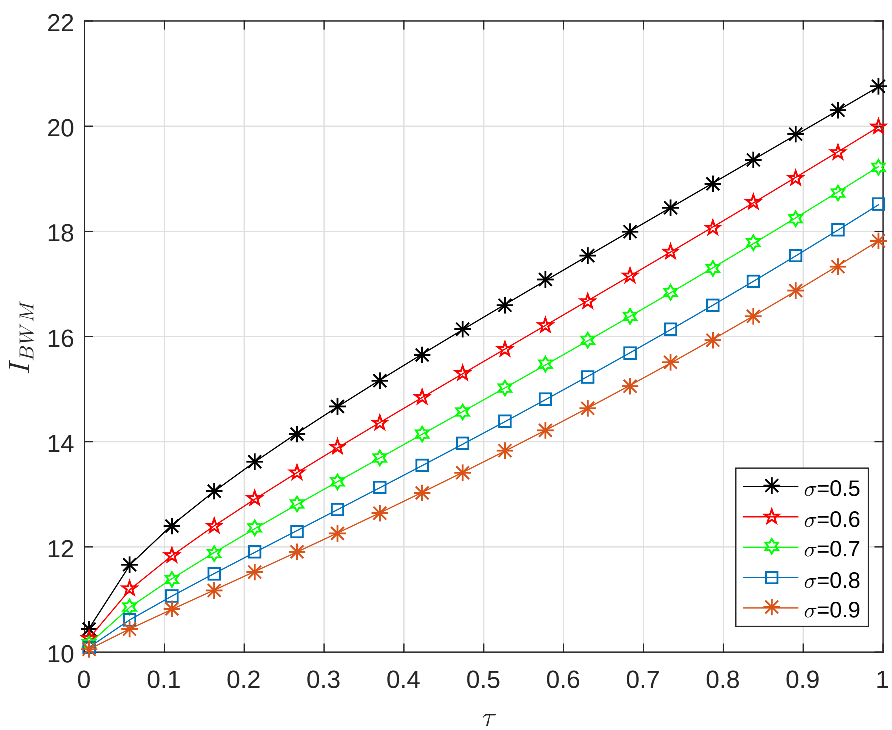

Figure 11. Behavior of Infected people w.r.t time for different values of σ.

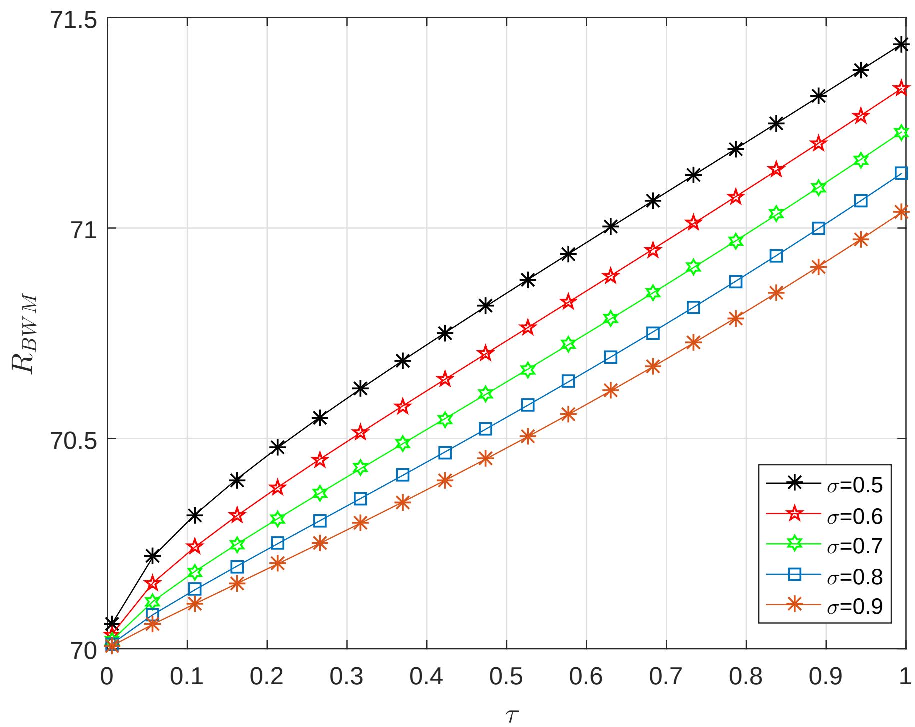

Figure 12. Behavior of Recovered people w.r.t time for different values of σ.

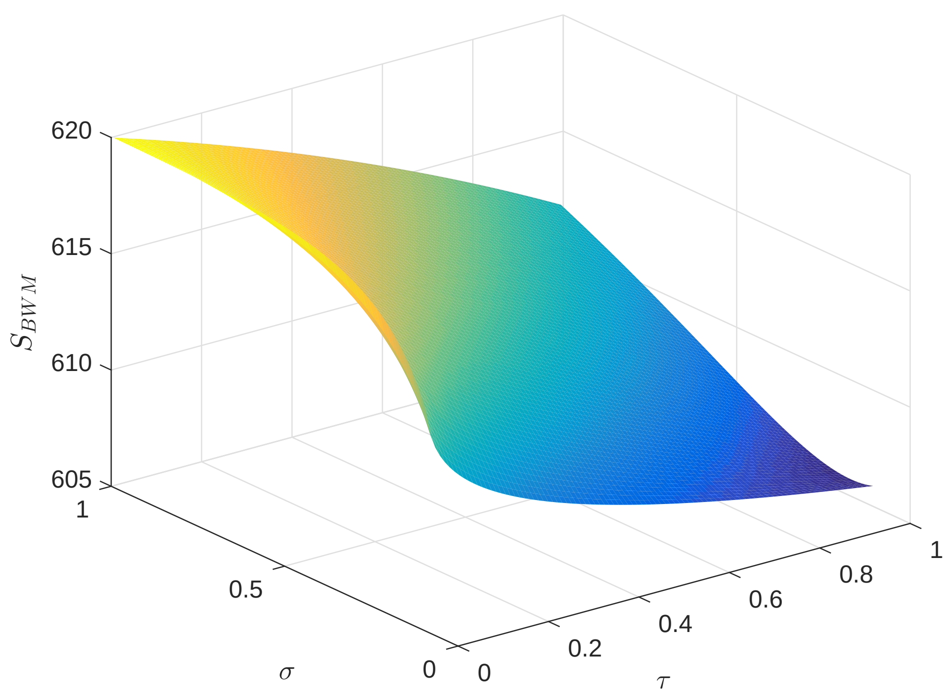

Figure 13. Behavior of Susceptible people w.r.t time and $0 < \sigma < 1$.

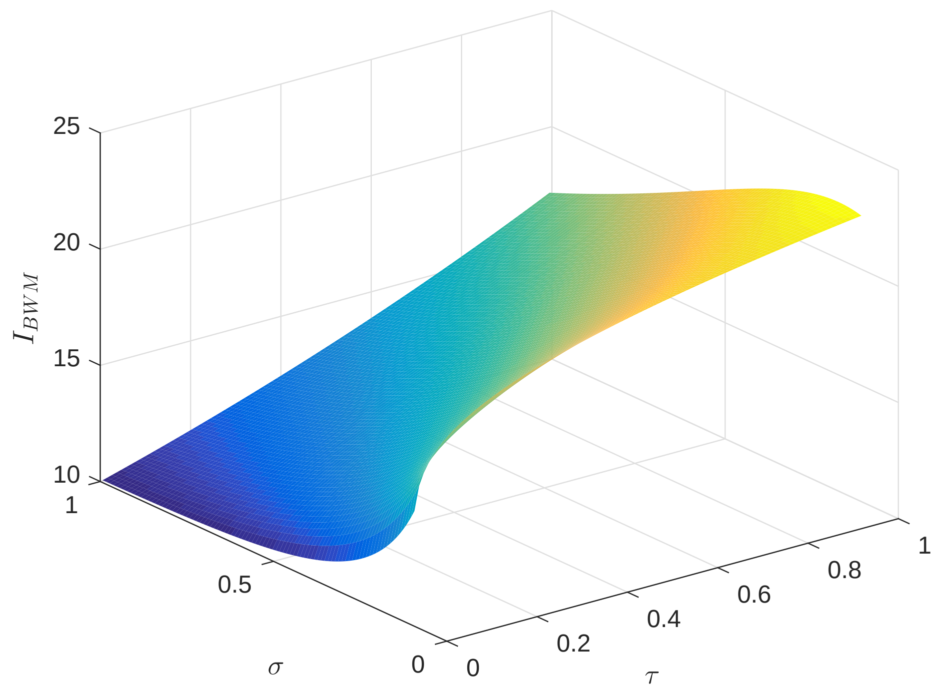

Figure 14. Behavior of Infected people w.r.t time and $0 < \sigma < 1$.

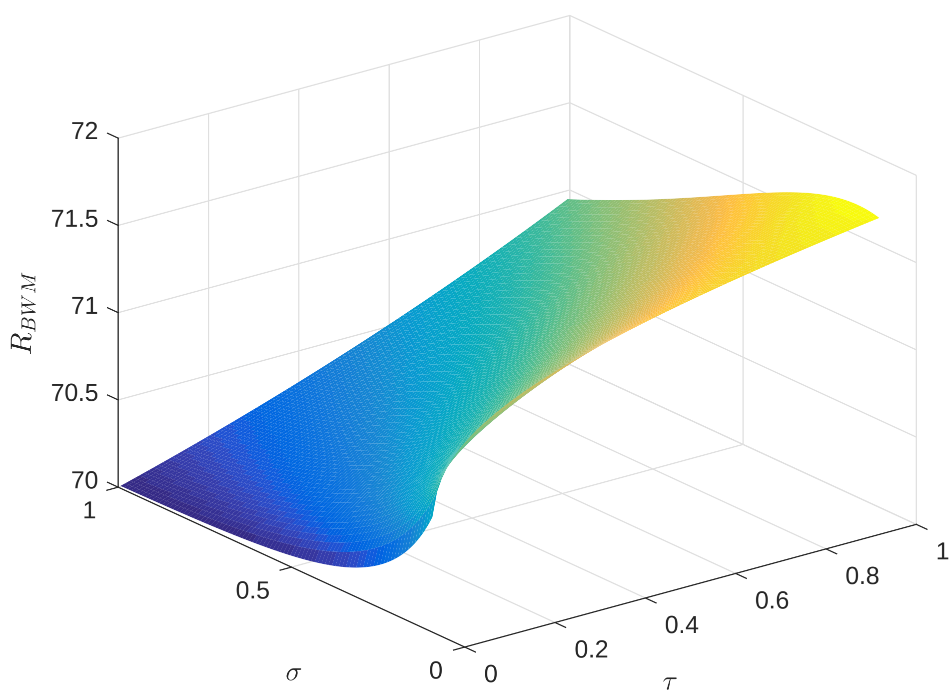

Figure 15. Behavior of Recovered people w.r.t time and $0 < \sigma < 1$.

Table 1. Comparison of solutions among proposed methods and other numerical methods for Susceptible people at $\sigma = 1$.

τ	S_{BWM}	S_{ABM}	$RK4$ [42]	RPS [42]
0.1	619.3630274221	619.3545091202	619.3630315796	619.3630315791
0.2	618.6909310646	618.6819439088	618.6909370609	618.6909370597
0.3	617.9818627742	617.9723821904	617.9818692109	617.9818692025
0.4	617.2338887502	617.2238890180	617.2338939798	617.2338939757
0.5	616.4449797181	616.4344339299	616.4449876950	616.4449876822
0.6	615.6130280833	615.6019081178	615.6130341588	615.6130341421
0.7	614.7358134999	614.7240899754	614.7358219653	614.7358219528
0.8	613.8110328171	613.7986750681	613.8110418712	613.8110418536
0.9	612.8362767043	612.8232527460	612.8362842538	612.8362842258

Table 2. Comparison of solutions among proposed methods and other numerical methods for Infected people at $\sigma = 1$.

τ	I_{BWM}	I_{ABM}	$RK4$ [42]	RPS [42]
0.1	10.5629635355	10.5704915979	10.5629598705	10.5629598709
0.2	11.1568872979	11.1648285758	11.1568820133	11.1568820144
0.3	11.7833906224	11.7917666401	11.7833849513	11.7833849586
0.4	12.4441667062	12.4529999757	12.4441620994	12.4441621031
0.5	13.1409910564	13.1503051108	13.1409840323	13.1409840435
0.6	13.8757061597	13.8855255736	13.8757008108	13.8757008253
0.7	14.6502515430	14.6606019698	14.6502440931	14.6502441041
0.8	15.4666371350	15.4775453242	15.4666291698	15.4666291853
0.9	16.3269635312	16.3384573546	16.3269568911	16.3269569155

Table 3. Comparison of solutions among proposed methods and other numerical methods for Recovered people at $\sigma = 1$.

τ	R_{BWM}	R_{ABM}	$RK4$ [42]	RPS [42]
0.1	70.0740090423	70.0749992818	70.0740085497	70.0740085498
0.2	70.1521816374	70.1532275152	70.1521809256	70.1521809257
0.3	70.2347466032	70.2358511694	70.2347458376	70.2347458387
0.4	70.3219445434	70.3231110062	70.3219439206	70.3219439211
0.5	70.4140292254	70.4152609591	70.4140282725	70.4140282742
0.6	70.5112657569	70.5125663085	70.5125663085	70.5112650324
0.7	70.6139349570	70.6153080546	70.613933941	70.6139339429
0.8	70.7223300477	70.7237796076	70.7223289588	70.7223289610
0.9	70.8367597643	70.8382898993	70.8367588550	70.8367588586

8. Conclusions

In this study, to get the numerical solutions of the non-linear fractional SIR epidemic model, a pattern of Bernstein wavelet method was discussed. In addition, an error estimation and convergence analysis of the function approximation based on aforesaid wavelets was discussed. Furthermore, an exact approximation for arbitrary order Riemann–Liouville integral operator was also discussed. The operational matrix together with collocation points was used to diminish the non-linear FDEs into several algebraic equations. Another numerical method known as Adams–Bashforth–Moulton was additionally discussed to show the precision and applicability of the suggested method. Convergence and error analysis assert the validity of proposed method.

Author Contributions: Conceptualization, S.K. and D.K.; methodology, R.K. and J.S.; software, R.K. and D.K.; validation, J.S., D.B. and M.S.; formal analysis, R.K. and D.K.; investigation, R.K. and A.A.; resources, S.K. and J.S.; data curation, S.K. and R.K.; writing—original draft preparation, S.K., R.K. and J.S.; writing—review and editing, A.A. and M.S.; visualization, D.B.; supervision, S.K. and D.B.; project administration, S.K. and D.B.; funding acquisition, S.K. and M.S. All authors have read and agreed to the published version of the manuscript.

Funding: This research was funded by SERB, Government of India, grant number EEQ/2017/000385.

Conflicts of Interest: The authors declare no conflict of interest.

References

1. Kermack, W.O.; McKendrick, A.G. A contribution to the mathematical theory of epidemics. *Proc. R. Soc. Lond. Ser. A Contain. Pap. Math. Phys. Character* **1927**, *115*, 700–721.
2. Ullah, S.; Khan, M.A.; Farooq, M. A new fractional model for the dynamics of the hepatitis B virus using the Caputo-Fabrizio derivative. *Eur. Phys. J. Plus* **2018**, *133*, 237. [CrossRef]
3. Cardoso, L.; Santos, F.D.; Camargo, R. Analysis of fractional-order models for hepatitis B. *Comput. Appl. Math.* **2018**, *37*, 4570–4586. [CrossRef]
4. Arafa, A.; Rida, S.; Khalil, M. Solutions of fractional order model of childhood diseases with constant vaccination strategy. *Math. Sci. Lett.* **2012**, *1*, 17–23. [CrossRef]
5. Shah, S.A.A.; Khan, M.A.; Farooq, M.; Ullah, S.; Alzahrani, E.O. A fractional order model for Hepatitis B virus with treatment via Atangana–Baleanu derivative. *Phys. A Stat. Mech. Its Appl.* **2020**, *538*, 122636. [CrossRef]
6. Singh, H.; Dhar, J.; Bhatti, H.S.; Chandok, S. An epidemic model of childhood disease dynamics with maturation delay and latent period of infection. *Model. Earth Syst. Environ.* **2016**, *2*, 79. [CrossRef]
7. Koca, I. Analysis of rubella disease model with non-local and non-singular fractional derivatives. *Int. J. Optim. Control Theor. Appl. (IJOCTA)* **2017**, *8*, 17–25. [CrossRef]
8. Rabi, F.A.; Al Zoubi, M.S.; Kasasbeh, G.A.; Salameh, D.M.; Al-Nasser, A.D. SARS-CoV-2 and Coronavirus Disease 2019: What We Know So Far. *Pathogens* **2020**, *9*, 231. [CrossRef]
9. Asgari, M.; Ezzati, R. Using operational matrix of two-dimensional Bernstein polynomials for solving two-dimensional integral equations of fractional order. *Appl. Math. Comput.* **2017**, *307*, 290–298. [CrossRef]
10. Mirzaee, F.; Samadyar, N. Numerical solution based on two-dimensional orthonormal Bernstein polynomials for solving some classes of two-dimensional nonlinear integral equations of fractional order. *Appl. Math. Comput.* **2019**, *344*, 191–203. [CrossRef]
11. Chen, Y.; Liu, L.; Li, B.; Sun, Y. Numerical solution for the variable order linear cable equation with Bernstein polynomials. *Appl. Math. Comput.* **2014**, *238*, 329–341. [CrossRef]
12. Razzaghi, M.; Yousefi, S. The Legendre wavelets operational matrix of integration. *Int. J. Syst. Sci.* **2001**, *32*, 495–502. [CrossRef]
13. Shamsi, M.; Razzaghi, M. Solution of Hallen's integral equation using multiwavelets. *Comput. Phys. Commun.* **2005**, *168*, 187–197. [CrossRef]
14. Lakestani, M.; Razzaghi, M.; Dehghan, M. Semi-orthogonal spline wavelets approximation for Fredholm integro-differential equations. *Math. Probl. Eng.* **2006**, *2006*. [CrossRef]
15. Beylkin, G.; Coifman, R.; Rokhlin, V. Fast wavelet transforms and numerical algorithms i. *Commun. Pure Appl. Math.* **1991**, *44*, 141–183. [CrossRef]
16. Iqbal, M.A.; Saeed, U.; Mohyud-Din, S.T. Modified Laguerre wavelets method for delay differential equations of fractional-order. *Egypt. J. Basic Appl. Sci.* **2015**, *2*, 50–54. [CrossRef]
17. Shiralashetti, S.; Kumbinarasaiah, S. Laguerre wavelets collocation method for the numerical solution of the Benjamina–Bona–Mohany equations. *J. Taibah Univ. Sci.* **2019**, *13*, 9–15. [CrossRef]
18. Gümgüm, S. Laguerre wavelet method for solving Troesch equation. *Balıkesir Üniversitesi Fen Bilimleri Enstitüsü Dergisi* **2019**, *21*, 494–502. [CrossRef]
19. Shiralashetti, S.; Angadi, L.; Kumbinarasaiah, S. Laguerre wavelet-Galerkin method for the numerical solution of one dimensional partial differential equations. *Int. J. Math. Appl.* **2018**, *6*, 939–949.

20. Shiralashetti, S.; Kumbinarasaiah, S. Theoretical study on continuous polynomial wavelet bases through wavelet series collocation method for nonlinear Lane–Emden type equations. *Appl. Math. Comput.* **2017**, *315*, 591–602. [CrossRef]
21. Wang, J.; Xu, T.-Z.; Wei, Y.-Q.; Xie, J.-Q. Numerical simulation for coupled systems of nonlinear fractional order integro-differential equations via wavelets method. *Appl. Math. Comput.* **2018**, *324*, 36–50. [CrossRef]
22. Yuttanan, B.; Razzaghi, M. Legendre wavelets approach for numerical solutions of distributed order fractional differential equations. *Appl. Math. Model.* **2019**, *70*, 350–364. [CrossRef]
23. Rahimkhani, P.; Ordokhani, Y. A numerical scheme based on Bernoulli wavelets and collocation method for solving fractional partial differential equations with dirichlet boundary conditions. *Numer. Methods Partial Differ. Equ.* **2019**, *35*, 34–59. [CrossRef]
24. Kumar, D.; Singh, J.; Qurashi, M.; Baleanu, D. A new fractional SIRS-SI malaria disease model with application of vaccines, anti-malarial drugs, and spraying. *Adv. Differ. Equ.* **2019**, *2019*, 278. [CrossRef]
25. Kumar, D.; Singh, J.; Baleanu, D. On the analysis of fractional diabetes model with exponential law. *Adv. Differ. Equ.* **2018**, *2018*, 231.
26. Goswami, A.; Singh, J.; Kumar, D. An efficient analytical approach for fractional equal width equations describing hydro-magnetic waves in cold plasma. *Physica A* **2019**, *2019*, 563–575. [CrossRef]
27. Srivastava, M.; Agrawal, S.; Das, S. Synchronization of chaotic fractional order Lotka–Volterra system. *Int. J. Nonlinear Sci.* **2012**, *13*, 482–494.
28. Diethelm, K.; Ford, N.J.; Freed, A.D. Detailed error analysis for a fractional Adams method. *Numer. Algorithms* **2004**, *36*, 31–52. [CrossRef]
29. Ghanbari, B.; Kumar, S.; Kumar, R. A study of behaviour for immune and tumor cells in immunogenetic tumour model with non-singular fractional derivative. *Chaos Soliton Fractals* **2020**. [CrossRef]
30. Kumar, S.; Nisar, K.; Kumar, R.; Cattani, C.; Samet, B. A new rabotnov fractional-exponential function based fractional derivative for diffusion equation under external force. *Math. Methods Appl. Sci.* **2020**. [CrossRef]
31. Kumar, S.; Kumar, R.; Singh, J.; Nisar, K.; Kumar, D. An efficient numerical scheme for fractional model of HIV-1 infection of CD4+ T-Cells with the effect of antiviral drug therapy. *Alex. Eng. J.* **2019**. [CrossRef]
32. Jleli, M.; Kumar, S.; Kumar, R.; Samet, B. Analytical approach for time fractional wave equations in the sense of Yang-Abdel-Aty-Cattani via the homotopy perturbation transform method. *Alex. Eng. J.* **2019**. [CrossRef]
33. Goufo, E.F.D.; Kumar, S.; Mugisha, S. Similarities in a fifth-order evolution equation with and with no singular kernel. *Chaos Solitons Fractals* **2020**, *130*, 109467. [CrossRef]
34. El-Ajou, A.; Oqielat, M.N.; Al-Zhour, Z.; Kumar, S.; Momani, S. Solitary solutions for time-fractional nonlinear dispersive PDEs in the sense of conformable fractional derivative. *Chaos Interdiscip. J. Nonlinear Sci.* **2019**, *29*, 093102. [CrossRef]
35. Kumar, S.; Kumar, A.; Momani, S.; Aldhaifallah, M.; Nisar, K.S. Numerical solutions of nonlinear fractional model arising in the appearance of the stripe patterns in two-dimensional systems. *Adv. Differ. Equ.* **2019**, *2019*, 413. [CrossRef]
36. Sharma, B.; Kumar, S.; Cattani, C.; Baleanu, D. Nonlinear dynamics of Cattaneo–Christov heat flux model for third-grade power-law fluid. *J. Comput. Nonlinear Dyn.* **2020**, *15*. [CrossRef]
37. Kudu, M. A parameter uniform difference scheme for the parameterized singularly perturbed problem with integral boundary condition. *Adv. Differ. Equ.* **2018**, *2018*, 1–12. [CrossRef]
38. Veeresha, P.; Prakasha, D.; Kumar, D. An efficient technique for nonlinear time-fractional Klein–Fock–Gordon equation. *Appl. Math. Comput.* **2020**, *364*, 124637. [CrossRef]
39. Bhatter, S.; Mathur, A.; Kumar, D.; Singh, J. A new analysis of fractional Drinfeld–Sokolov–Wilson model with exponential memory. *Phys. A Stat. Mech. Its Appl.* **2020**, *537*, 122578. [CrossRef]
40. Choudhary, A.; Kumar, D.; Singh, J. Numerical simulation of a fractional model of temperature distribution and heat flux in the semi infinite solid. *Alex. Eng. J.* **2016**, *55*, 87–91. [CrossRef]

41. Ghanbari, B.; Kumar, D. Numerical solution of predator-prey model with Beddington-DeAngelis functional response and fractional derivatives with Mittag-Leffler kernel. *Chaos Interdiscip. J. Nonlinear Sci.* **2019**, *29*, 063103. [CrossRef] [PubMed]
42. Hasan, S.; Al-Zoubi, A.; Freihet, A.; Al-Smadi, M.; Momani, S. Solution of fractional SIR epidemic model using residual power series method. *Appl. Math.* **2019**, *13*, 1–9. [CrossRef]